Electronic Supplementary Information

Highly dispersed Ru clusters toward efficient and durable hydrogen oxidation reaction

Ge Meng et al.

Experimental Section

Preparation of NHCS, Ru_p/NHCS and Ru_c/NHCS

According to the literature,[30] $Zn(NO_3)_2 \cdot 6H_2O$ (225 mg) with ferroceneboronic acid (46 mg), and 2-methylimidazole (2.75 g) were dissolved in deionized water (7.5 mL), respectively. The two solutions were mixed quickly. The ZIF-8 polyhedrons was obtained by stirring for 6 h at room temperature (RT). Then, 200 mg ZIF-8 powder was mixed with 100 mg dopamine hydrochloride in a 50 mL Tris aqueous solution under magnetic stirring for 24 h to yield ZIF-8@PDA. Subsequently, 100 mg ZIF-8@PDA was added into $Ru(acac)_3$ solution (0.1 mmol) and stirring for 2 h at RT. Finally, the obtained ZIF-8@PDA@$Ru(acac)_3$ precipitates were heated to 800 ^oC for 2 h to generate Ru_c/NHCS. Similarly, the control samples (Ru_p/NHCS and NCHS) were prepared via an identical synthesis route but with 0.3 mmol $Ru(acac)_3$ and without $Ru(acac)_3$ addition, respectively.

Characterizations

The morphology of the prepared samples were characterized by SEM (Quanta FEG 250) and TEM (Talos F200X), respectively. The crystalline structures were analyzed by Rigaku D/max 2500 X-ray diffractometer (XRD) with Cu Kα radiation (λ = 0.154598 nm). X-ray photoelectron spectroscopy (XPS, ESCALAB 250Xi, Thermo Scientific) was acquired with a monochromatic Al Kα radiation source.

HOR measurements

All electrochemical tests were carried out on an electrochemical workstation (CHI 760E) with a standard three-electrode system with the 0.1 M KOH solution as the electrolyte at 25°C. A graphite rod and Hg/HgO electrode were applied as the counter electrode and reference electrode, respectively. The glassy carbon electrode loading catalyst inks were performed as

the working electrode. To prepare the catalyst ink, 5 mg of the sample was dispersed in a solution containing 500 μL 0.5 wt.% Nafion and 500 μL ethanol, and then the ink was dispersed by ultrasound for at least 30 min. After that, the ink was dropped at the glassy carbon electrode (0.196 cm^{-2} for the active geometric area) and dried in room temperature. The catalyst loading of Ru_c/NHCS on the glassy carbon electrode was 0.2 mg cm^{-2}. As a comparison, the NCHS, Ru_p/NHCS and Pt/C electrodes were also measured. *i*R compensation was applied to all initial data except stability data. All the potential values were calculated according to the equation, $E_{RHE} = E_{Hg/HgO} + E^{o}_{Hg/HgO} + 0.059$ pH. Copper underpotential deposition (Cu-UPD) stripping measurement was conducted in an Ar-purged 0.5 M H_2SO_4 solution containing 5 mM of $CuSO_4$ after Cu deposition at 0.276 V for 100 s.

AEMFC test

Based on the literature,[2,20] catalyst ink was prepared by mixing catalyst with 5 wt% Nafion ionomers diluted by isopropanol/water (1 : 1) solvent. The catalyst ink was ultrasonic treated for 1 hour and sprayed on two side of Gore ionomer membrane (20 μm) with an effective area of 4 cm^2 using airbrush (S130). The Ru_p/NHCS, Ru_c/NHCS, and 20 wt% Pt/C (JM) were used as anode with a metal loading of 24 μg_{metal} cm^{-2}, while the commercial Pt/C was used as cathode with a loading of 100 μg_{Pt} cm^{-2}. Then we tested them using Scribner 850e as condition-controlled fuel cell test station at 80 ^{o}C and 100% relative humidity. The back pressures and gas flow rates were set to 2 atm and 300 mL min^{-1}, respectively.

DFT calculations

To investigate the HOR performance of Ru clusters and comparative samples, all theoretical studies were performed using the Dmol^3 program in Materials Studio. Here, for Comparison of Ru metal and Pt/C, using representative crystal planes Ru (001) and Pt (111) in the calculations were to study their HOR performances. During the calculation process, based on

density functional theory (DFT), the Perdew-Burke-Ernzerhof (PBE) functional with the generalized gradient approximation (GGA) was adopted. To avoid periodic action of each structure in the z direction, the vacuum layers of all structures accompanied with spin-polarized were larger than 15 Å. To calculate the Gibbs free energy change in the HOR path, each value of change (ΔG) was determined according to the computational hydrogen electrode (CHE) model by:

$$\Delta G = \Delta E_{ads} - T\Delta S + ZPVE + \int C_{\mathrm{p}}\,\mathrm{d}T$$

in the above physical symbols, where ΔE_{ads} represents energy difference changed by adsorbate, and ΔS and $ZPVE$ are entropy difference and zero-point vibrational energy, respectively. T and C_p represent temperature around system and thermal capacity, respectively. While the vibrational enthalpy and entropy contributions of absorbed species are negligible according to previous theoretical studies.

Figures and Table

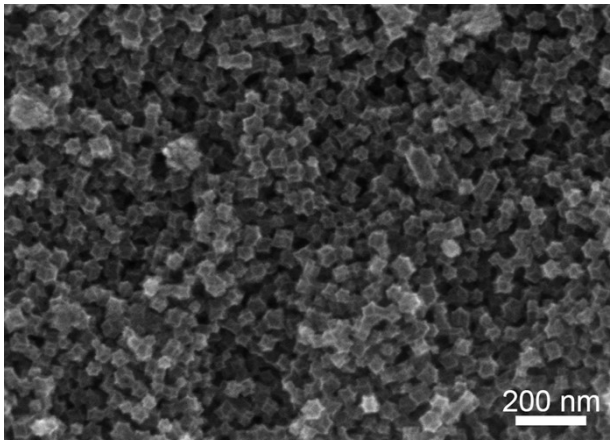

Figure S1. SEM image of the as-prepared ZIF-8 polyhedrons.

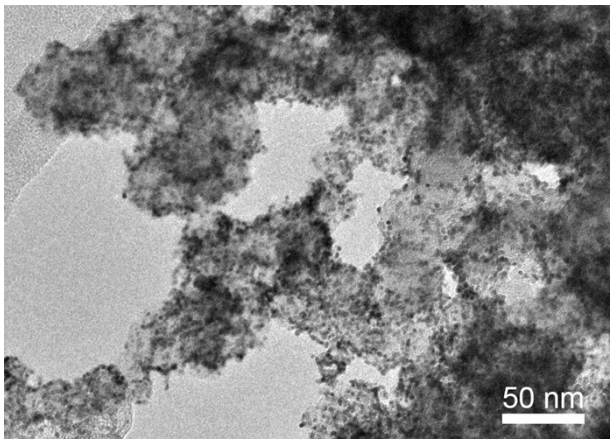

Figure S2. TEM image of the as-prepared Ru_p/NCHS. Clearly, Ru particles spread throughout the hollow carbon spheres.

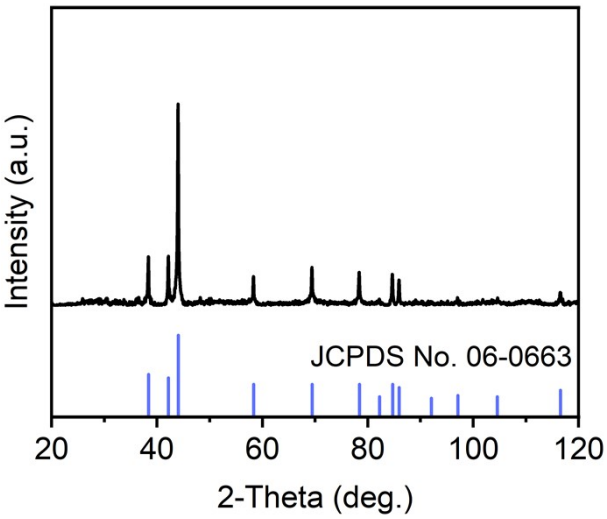

Figure S3. XRD pattern of the as-prepared Ru_p/NCHS. All the diffraction peaks can be ascribed to hexagonal phase of Ru (JCPDS No. 06-0663).

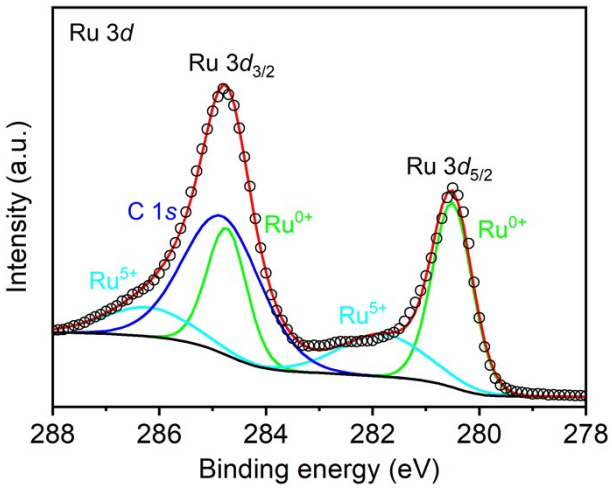

Figure S4. High-resolution Ru 3*d* XPS spectrum of the as-prepared Ru_p/NCHS. The peaks in Ru_p/NCHS can be deconvoluted into two Ru $3d_{5/2}$ peaks at 280.5 and 281.2 eV, which correspond to Ru^0 and Ru^{5+}, respectively (*Nano Energy* 2021, 88, 106211). Similarly, the twao Ru $3d_{3/2}$ peaks at 284.7 and 286.2 eV can be ascribed to Ru^0 and Ru^{4+}, respectively. Of note, the XPS result confirms that metallic Ru^0 is dominant over the positive charged Ru species, which is consistent with XRD pattern (Figure S3).

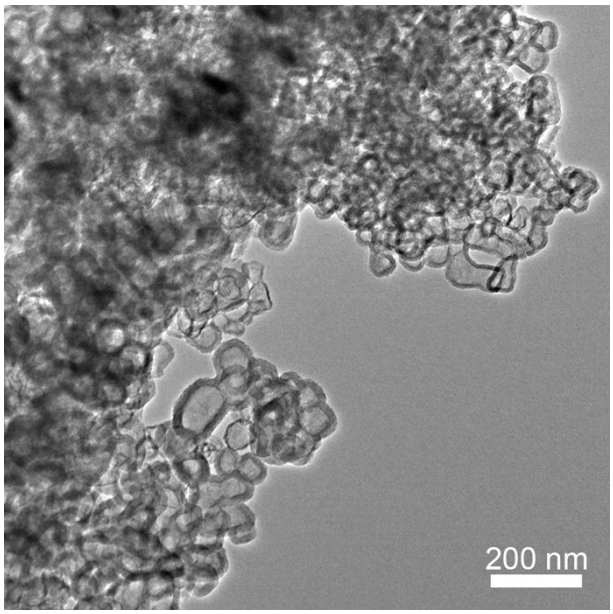

Figure S5. TEM image of the as-prepared NCHS.

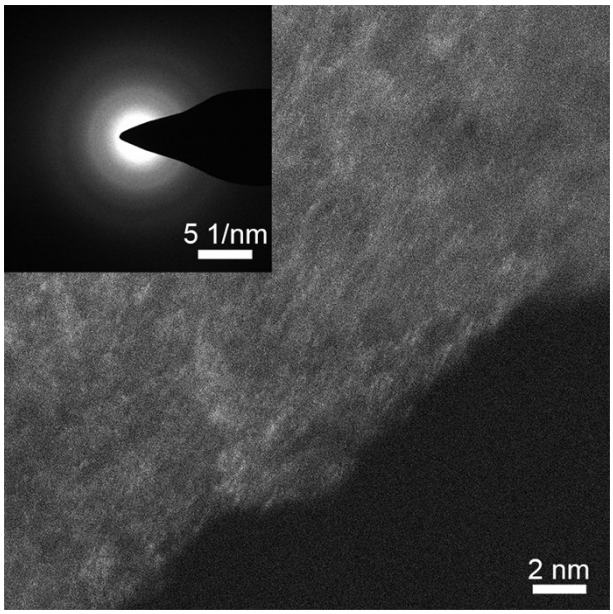

Figure S6. HRTEM image of the carbon shell of the as-prepared NCHS (inset shows the corresponding selected area electron diffraction (SAED) pattern). Here, the lattice fringe of carbon cannot be detected due to its amorphous nature, which is further confirm by SAED.

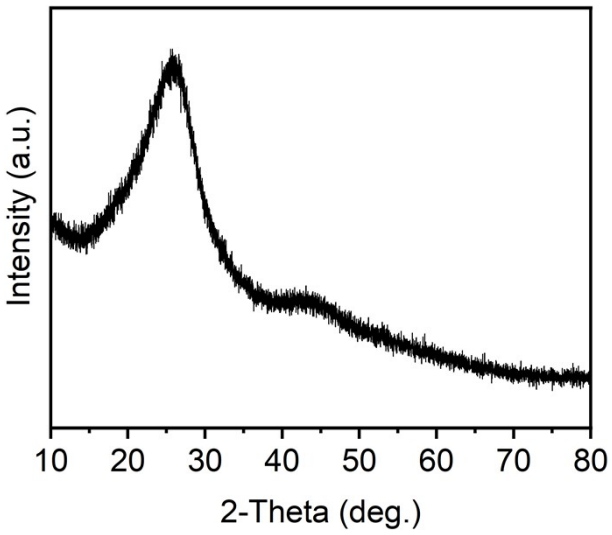

Figure S7. XRD pattern of the as-prepared Ru_c/NCHS.

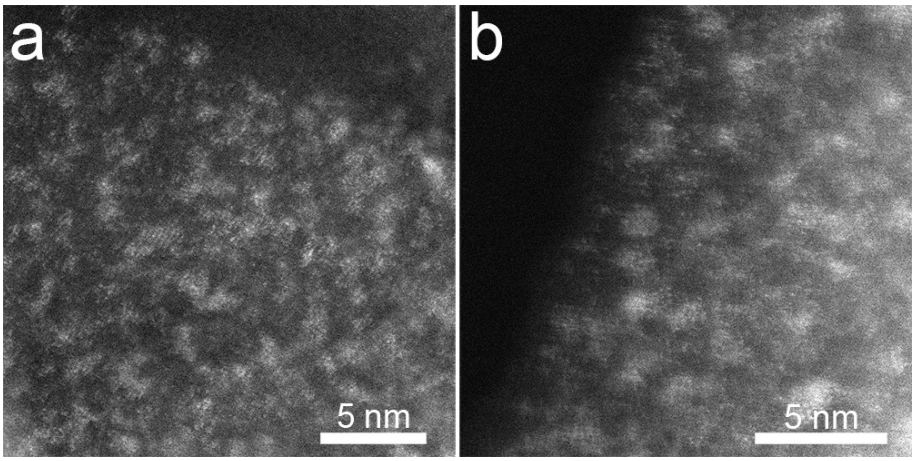

Figure S8. HAADF-STEM images of the as-prepared Ru_c/NCHS.

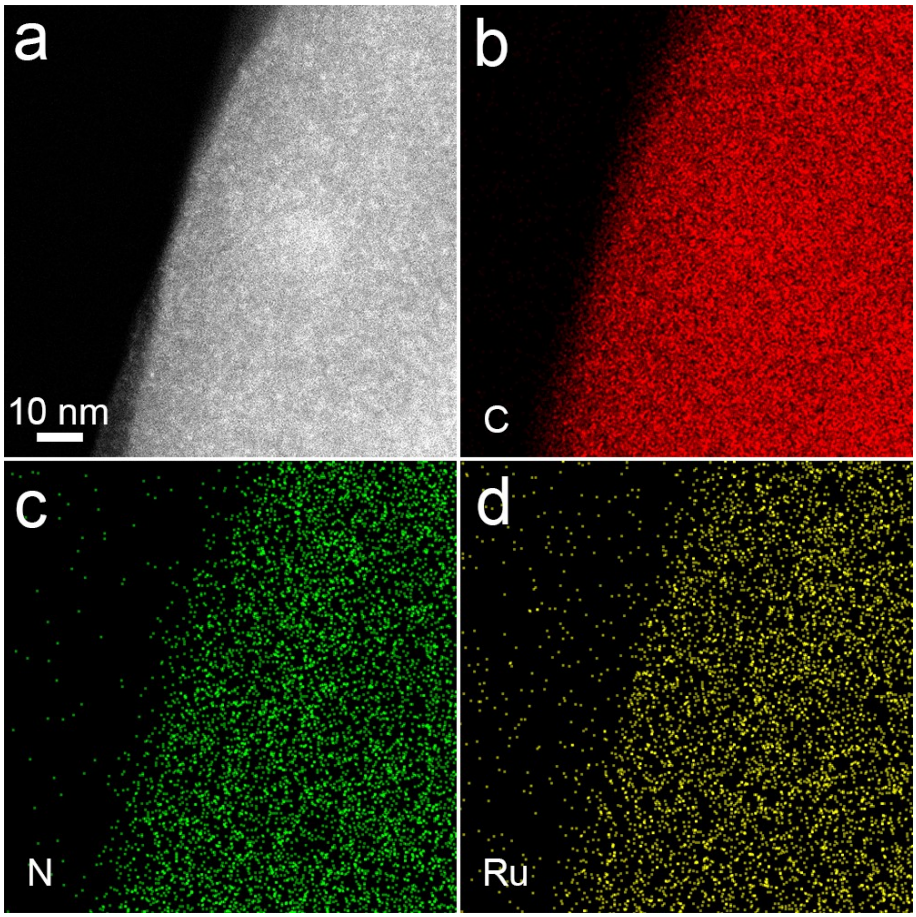

Figure S9. Elemental mappings of the as-prepared Ru_c/NCHS.

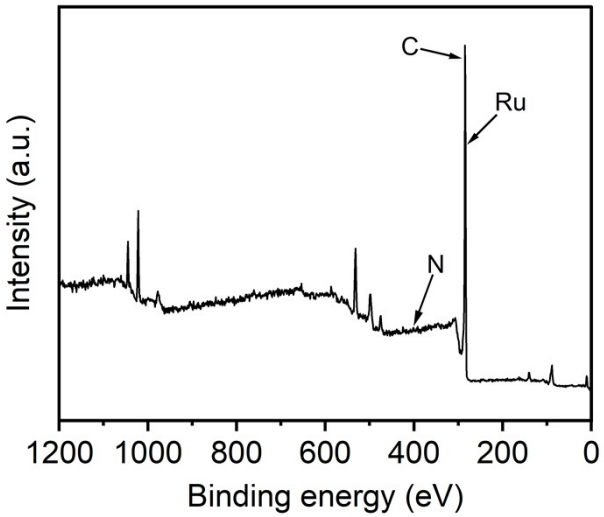

Figure S10. XPS survey spectrum of the as-prepared Ru_c/NCHS.

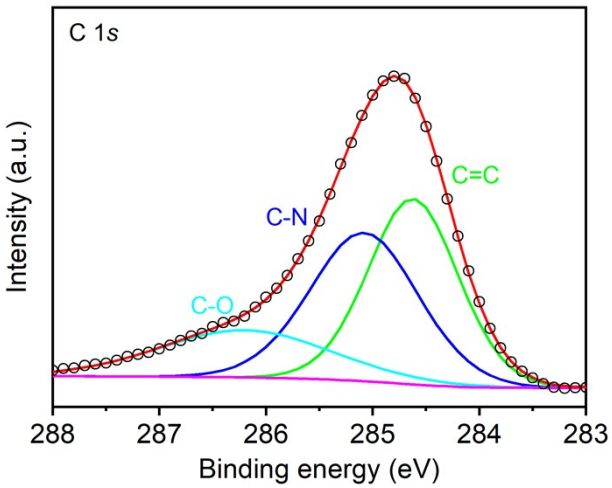

Figure S11. High-resolution C 1*s* XPS spectrum of the as-prepared Ru_c/NCHS. The C 1s XPS spectrum demonstrates the existence of C=C (284.6 eV), C–O (286.2), and C=N (285.1 eV) bonds in Ru_c/NCHS (*iScience* 2020, 23, 101793).

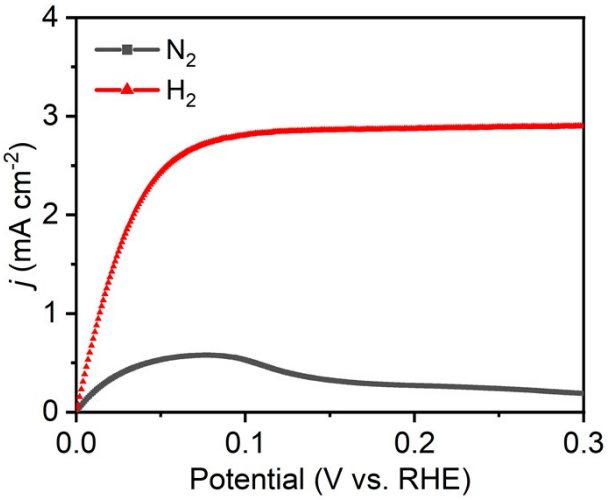

Figure S12. HOR polarization curves of the as-prepared Ru_c/NCHS recorded in Ar-/H_2-saturated electrolytes.

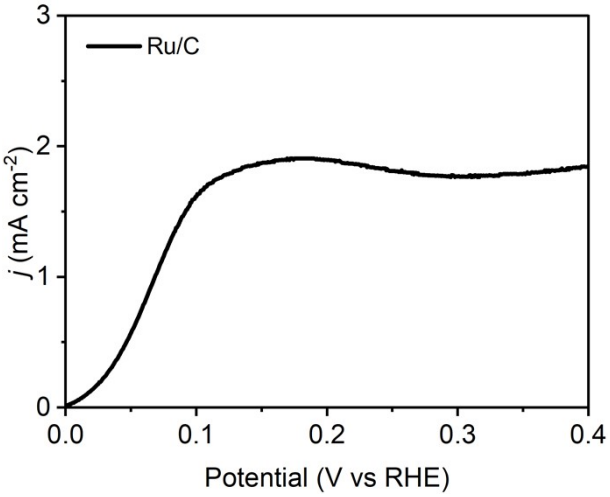

Figure S13. HOR polarization curves of the 20 wt% Ru/C recorded in H_2-saturated 0.1 M KOH solution. the HOR current density increases up to 0.2 V and then decreases. It is worth noting that the oxidation of Ru-species would happen when the potential is positive than 0.2 V (*J. Am. Chem. Soc.* 2013, 135, 8016). Interestingly, this self-oxidation can not observed on Ru_c/NCHS, suggesting the electrochemical superiority of our designed catalyst.

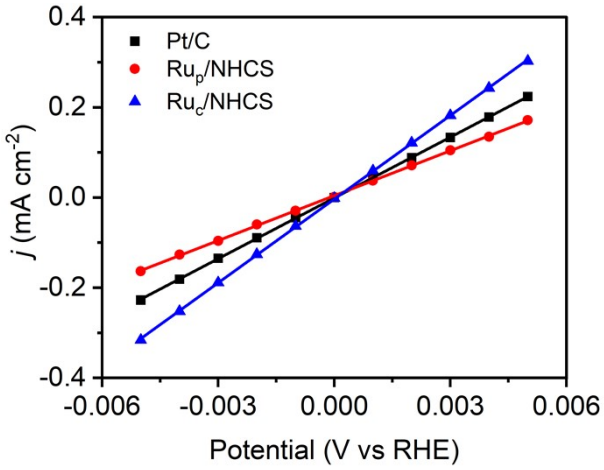

Figure S14. Micro-polarization region.

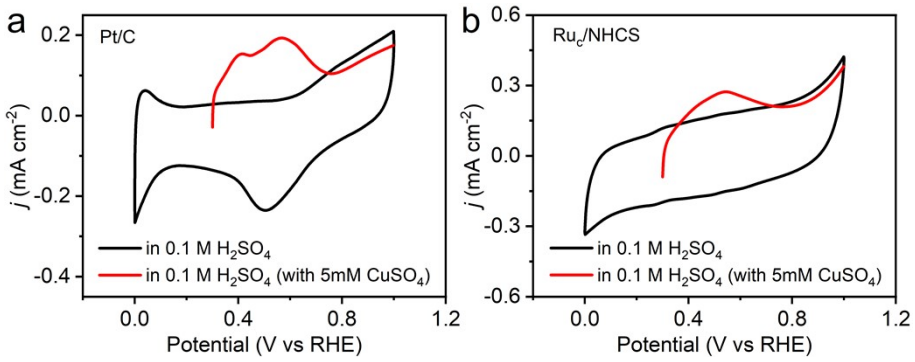

Figure S15. Cu-UPD measurements on Ru_c/NCHS and Pt/C. The measured ECSA for Ru_c/NCHS and Pt/C is 0.73 cm^2 μg_{Pt}^{-1} and 3.62 cm^2 μg_{Ru}^{-1}, respectively. It should be noted that the obtained ECSA on Pt/C is consistent with the literature (Zhao et al. ACS Catal. 2020, 10, 11751), indicative of the reliability of our measurements.

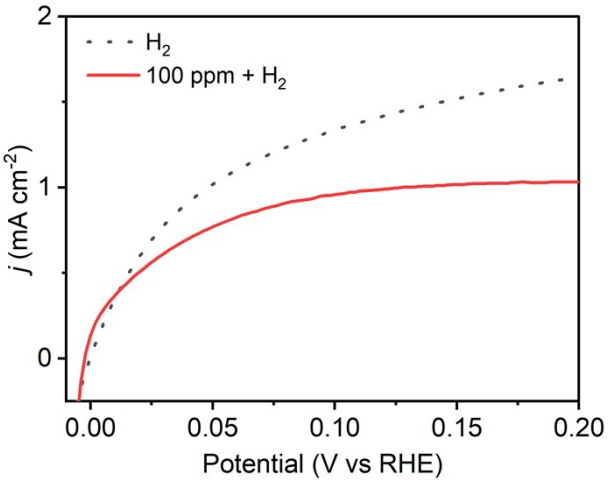

Figure S16. HOR polarization curves of Ru_p/NCHS recorded in electrolytes with (solid line) and without (dashed line) the addition of 100 ppm CO. It can be found that Ru_p/NCHS deliver a notable activity decay in H_2 with 100 ppm CO, implying its poor CO resistance.

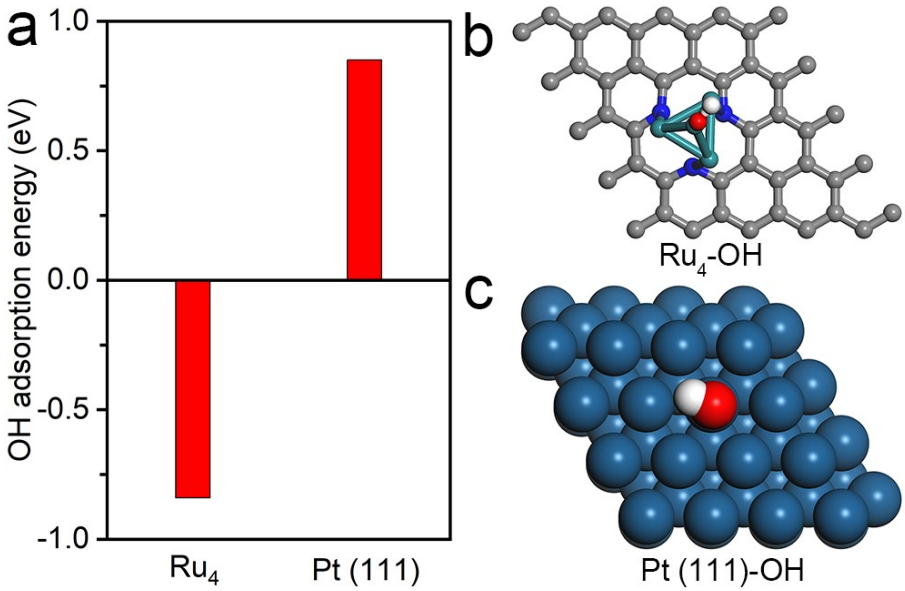

Figure S17. DFT calculated OH adsorption energies on Ru_p/NCHS, Ru_c/NCHS and Pt/C.

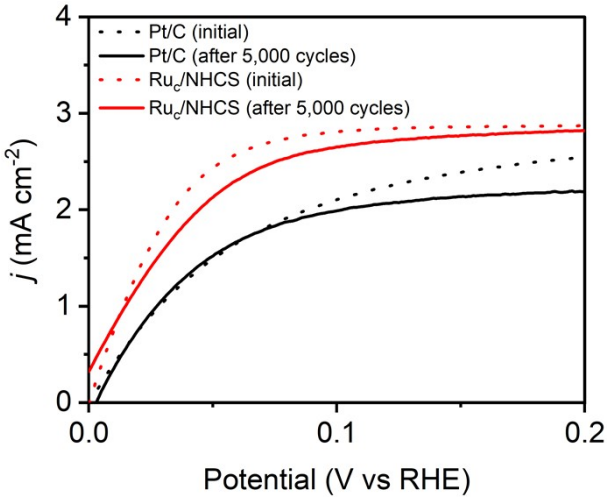

Figure S18. HOR polarization curves for Ru_c/NCHS and Pt/C recorded after 5,000 cyles.

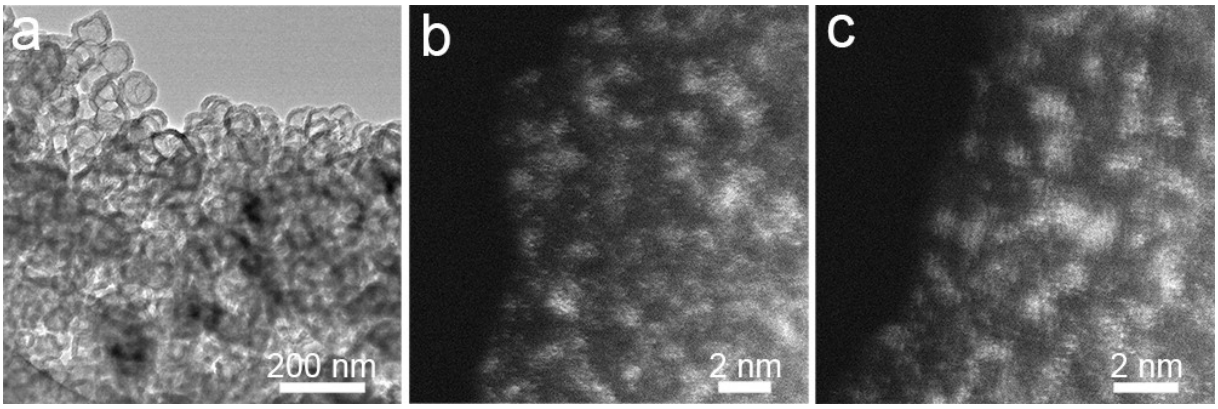

Figure S19. Additional TEM and HAADF-STEM images for Ru_c/NCHS after the 15-h electrolysis.

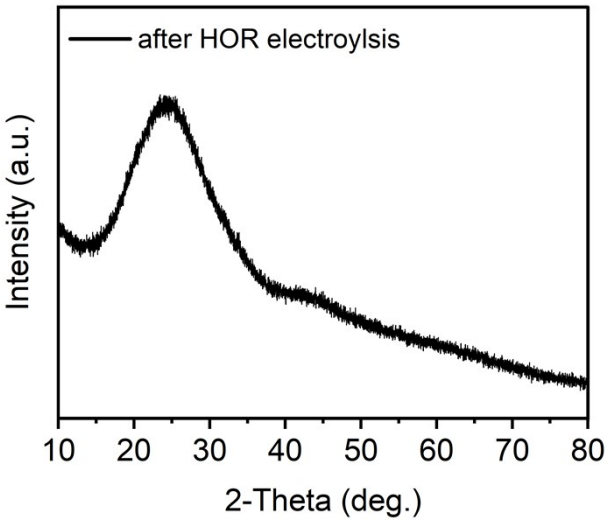

Figure S20. Additional XRD patterns of Ru_c/NCHS after the 15-h electrolysis. Clearly, no additional peaks can be observed after the stability test.

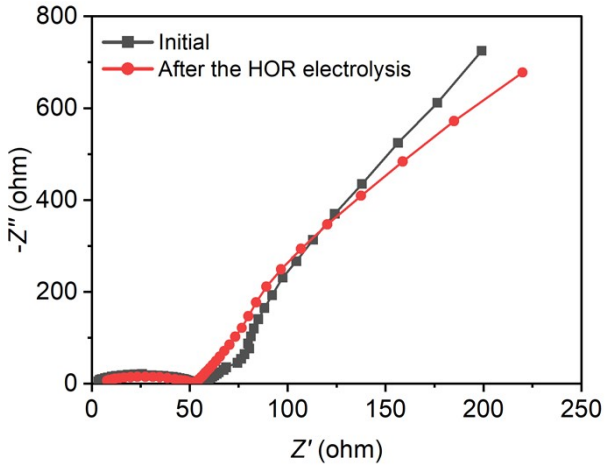

Figure S21. Additional impedance spectra of Ru_c/NCHS after the 15-h electrolysis. Clearly, the obtained two spectra are close to each other, indicative of the good electrochemical stability of Ru_c/NCHS.

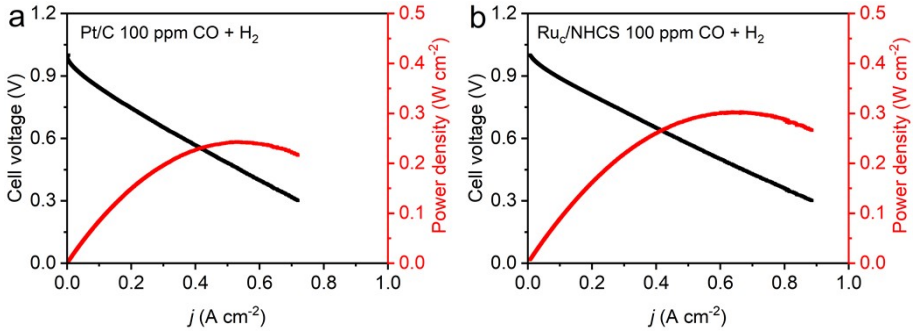

Figure S22. PEMFC cell performance of Ru_c/NCHS and Pt/C in H_2/100 ppm CO.